appliedoptics

LED nonlinearity mitigation in LACO-OFDM optical communications based on adaptive predistortion and postdistortion techniques

MOHAMMED ABD ELKARIM,[1,2] MOUSTAFA H. ALY,[3,*] HALA M. ABDELKADER,[1] AND M. M. ELSHERBINI[1,4]

[1]Department of Electrical Engineering, Shoubra Faculty of Engineering, Benha University, Cairo 11629, Egypt
[2]Department of Electronics and Communications, Modern Academy for Engineering and Technology, Cairo 11585, Egypt
[3]College of Engineering and Technology, Arab Academy for Science &Technology & Maritime Transport, Alexandria 21937, Egypt
[4]Department of Electrical Engineering, the Egyptian Academy of Engineering and Advanced Technology (EAEAT), Cairo, Egypt
*Corresponding author: mkarim.aysh@gmail.com

The preinstalled white light emitting diodes (WLEDs) inside buildings can be exploited as an optical source in visible light communications (VLC) motivated by high optical efficiency and low cost. One of the main challenges for VLC is LED nonlinear distortion, which has a detrimental effect on system performance. Estimation and compensation of the LED nonlinear behavior can be accomplished using predistortion or postdistortion techniques. Three compensation techniques are adopted to mitigate the effect of LED nonlinearity on layered asymmetrically clipped optical, orthogonal frequency division multiplexing. Their performance and efficiency are discussed and compared with the aid of error vector magnitude and bit error rate (BER) in an additive white Gaussian noise channel. The obtained results reveal that polynomial-based predistorters and postdistorters can overcome the LED nonlinear behavior with extra SNR of only 0.25 dB at BER of 10^{-3}. Furthermore, the look-up-table-based predistorter can provide the same BER with lower SNR penalty than the previous two systems. © 2021 Optical Society of America

https://doi.org/10.1364/AO.432364

1. INTRODUCTION

White light emitting diodes (WLEDs) are strongly nominated for short-range indoor optical wireless data transmission motivated by low power consumption, cost effectiveness, high output brightness, and long lifetime. Visible light communications (VLC) utilize WLEDs as an optical source shifting the communication range towards the visible light band with its unique features including huge and unregulated bandwidth and signal confinement within rooms. Also, it is preferable to radio frequency (RF)-based systems in some locations, where the use of the RF spectrum is not appropriate as in hospitals and aircrafts or even underwater data communications [1].

Orthogonal frequency division multiplexing (OFDM) was adopted in VLC systems as an efficient technique to provide high data rates and combat the problem of inter-symbol interference (ISI) resulting from intensive reflections from walls, ceiling, floor, and objects within the room [2]. OFDM systems are able to alleviate the problem of ISI, as the symbol duration is longer than the delay spread caused by multipath reflections. Additionally, OFDM has the advantage of utilizing single-tap equalizers at the receiver (Rx) to extract the original message. Instead of single carrier modulation techniques such as on–off keying (OOK) or pulse position modulation (PPM), OFDM

boosts the transmission capacity of the channel through parallel transmission of a large number of orthogonal subcarriers with high-order quadrature amplitude modulation (QAM) [3].

Conventional OFDM signals are complex and bipolar, bearing in mind that VLC accommodate intensity modulation and direct detection (IM/DD) due to its simplicity and low cost. IM/DD requires the signal to be real and nonnegative. Thus, a number of modifications are applied to the conventional OFDM to cope with IM/DD requirements. Such modifications lead to variants of optical OFDM systems. At the top of these systems are the DC-biased optical OFDM (DCO-OFDM) and asymmetrically clipped optical OFDM (ACO-OFDM). In DCO-OFDM, the odd- and even-indexed data subcarriers are constrained to the Hermitian symmetry (HS) at the input of the inverse fast Fourier transform (IFFT). Then, a DC level is added to the real output OFDM symbol to push the signal towards nonnegative values. In ACO-OFDM, only the odd-indexed data subcarriers are constrained to the HS, while the even-indexed ones are left unused. The ACO-OFDM symbol follows a half-wave symmetry and allows clipping at zero level without the need for an additional DC level. Thus, it is more power efficient than DCO-OFDM at the expense of the transmitted bit rate [3].

LED is a non-ohmic device and exhibits a nonlinear relationship between the driving current and the radiated optical power ($L - I$), as the number of emitted photons is not proportional to the injected current. This phenomenon causes harmonics at higher frequencies, which interfere with the transmitted signal and give rise to intermodulation products at different subcarriers.

Also, double-sided clipping of the signals beyond the dynamic range of LED operation [below the turn-on voltage (TOV) or signals higher than the maximum permissible AC/pulsed current] is a critical source of distortion and affects the overall system performance, especially for OFDM signals characterized by a high peak-to-average-power ratio (PAPR) resulting from the superposition of a large number of statistically independent subcarriers that can constructively sum up to high signal peaks in the time domain [4,5].

A. Related Work

A number of literatures have investigated and analyzed the detrimental effect of LED nonlinearity on the performance of optical OFDM systems. In [6,7], the authors investigated the effect of LED nonlinearity on discrete multitone modulation, approximating the LED behavior using a second-order polynomial equation and assuming a static transfer function. The presented study took into consideration the number of subcarriers, modulation index, modulation order, and the nonlinearity degree of the LED. Elgala et al. [8] modeled LED nonlinearity using the Rapp model and illustrated the effect of different model parameters on the system symbol error rate. The same authors investigated the effect of LED nonlinearity on DCO-OFDM considering different bias points and signal power values in [9].

Using a practical LED model, a comparison between ACO-OFDM and DCO-OFDM performances under LED nonlinearity and clipping distortion was conducted in [4,10], showing system performance at different power regions in an additive white Gaussian noise (AWGN) channel. In addition, both systems' performances under the clipping distortion were fully investigated in [11], taking into consideration both average optical power and dynamic optical power constraints comparing their error vector magnitude (EVM), signal-to-distortion ratio, and achievable data rates. A complete modeling of LED nonlinearity and clipping noise on DCO-OFDM, ACO-OFDM, pulse amplitude modulation (PAM)-OFDM, and unipolar orthogonal frequency division multiplexing (U-OFDM) was presented in [12]. A closed-form analytical expression was provided for the system bit error rate (BER) assuming a memoryless nonlinear distortion.

LED nonlinearity effects can be alleviated through linearization of the LED characteristics using predistortion or postdistortion. In predistortion, the LED nonlinear characteristics are first estimated at the transmitter side to compensate for LED nonlinearity. In postdistortion, the Rx applies the opposite function to the received data to retrieve the original data. There are several literatures that present and propose various predistortion and postdistortion techniques to combat LED nonlinearity.

In [13], using curve fitting, the LED model was first defined, followed by obtaining the predistorter coefficients such that the overall response of the system is linear. Approximating LED nonlinearity using the Weiner model, a postdistorter was proposed by Qian et al. [14] to combat LED nonlinearity with memory effects modeling the ($I - V$) characteristic using the Rapp model. An adaptive normalized least mean square (NLMS) algorithm was presented by J. Kim et al. [15] to track and compensate for the distortion caused by LED nonlinearity. Also, Li et al. [16] designed an adaptive nonlinear time-domain equalizer whose coefficients could be estimated using the LMS algorithm to compensate for the nonlinear distortion imposed by the LED. Also, in [17], P. Aggarwal et al. proposed and discussed an adaptive predistorter whose coefficients could be calculated using the least square (LS) method.

Chebyshev polynomial expansion was adopted in [18] as a predistortion technique to obtain the inverse of LED nonlinearity characteristics and mitigate its effect. A comparative study with the NLMS-based predistorter and Volterra-based postdistorter was presented to check its validity. Sheu et al. [19] combined the advantage of linearizing LED characteristics using a look-up table (LUT)-based predistorter with a PAPR reduction technique through applying a precoding matrix to the input signal at the IFFT stage. In [20], the authors combined the advantages of both predistortion and companding techniques to counteract the ($L - I$) and ($I - V$) nonlinear effects, respectively.

Chen et al. [21] proposed a nonlinearity estimation and compensation method based on probabilistic Bayesian learning for spectral-efficient VLC. Finally, there are a number of machine learning algorithms that are discussed to mitigate the LED nonlinearity including the k-means algorithm [22,23] and neural networks [24,25].

B. Contribution

In [5], the performance of the layered ACO-OFDM (LACO-OFDM) was investigated under the effect of LED nonlinearity and clipping distortion assuming four-layer LACO-OFDM utilizing a realistic LED model. A distinct treatment between the clipping noise and LED nonlinearity distortion was introduced to allow a detailed analysis for both problems. A comprehensive study on the effect of second-order nonlinear effects on the system was performed assuming an AWGN channel. The study took into account the transmission power, number of layers, severity of nonlinearity, and the modulation order. Additionally, a comparative study with conventional ACO-OFDM was presented. This paper extends the previous work and discusses how to overcome the problem of LED nonlinearity; the major contributions made in this paper are summarized as follows.

1. It is the first of its kind that discusses various techniques to combat the adverse effect of LED nonlinearity in four-layer LACO-OFDM and enhances the overall system performance assuming a realistic LED model with strong nonlinear characteristics.

2. Two predistortion techniques to combat LED nonlinearity are described and discussed. The first one determines the coefficients of the predistorter based on the LS method, where the inverse of the LED characteristics is a polynomial. The other is based on LUT, which stores the input–output pairs of LED nonlinearity and predistorts

the transmitted signal by assigning the input signal to the nearest member in the LUT.

3. On the other side, another nonlinearity compensation approach based on an adaptive postdistortion technique is evaluated and tested. The coefficients of postdistortion are calculated using the LS-method, where the inverse of the LED characteristics is a polynomial.

4. A complete analysis regarding the impact of input signal power and DC-bias voltage is presented and discussed. The optimum points for operation are found in each case. The aforementioned compensation techniques are discussed and evaluated in terms of EVM, BER, and BER penalty.

The remainder of this paper is organized as follows. Section 2 describes the operation of LACO-OFDM system with a complete description of the LED model. The evaluation process concerning the effect of LED nonlinearity, DC-bias voltage, and signal power is explained in Section 3. Predistortion techniques with a complete evaluation of their operation are provided in Sections 4 and 5, while the postdistortion technique is discussed and evaluated in Section 6. Section 7 is devoted to the main conclusions.

2. OPERATION OF LACO-OFDM

In conventional ACO-OFDM, the input bit stream is mapped into one of the complex values corresponding to one of the M-ary quadrature amplitude modulation (M-QAM) constellation points. Then, the complex-valued symbols are applied to the IFFT input following HS constraints such that the even data, zero, and N/2 subcarriers are left unmodulated, and the odd data subcarriers are modulated, such that [26]

$$X(k) = X^*(N - K), \quad k = 1, 3, \ldots, \frac{N}{2} - 1, \quad \textbf{(1)}$$

where $(.)^*$ denotes the complex conjugate, and N is the total number of data subcarriers. The output of the IFFT stage follows a half-wave symmetry, such that [26]

$$x(n) = -x\left(n + \frac{N}{2}\right), \quad n = 0, 1, 2, \ldots, \frac{N}{2} - 1. \quad \textbf{(2)}$$

Thus, the negative part can be clipped without loss of information, and the generated ACO-OFDM symbol is given by [26]

$$x_{ACO}(n) = \begin{Bmatrix} x(n), & x(n) \geq 0 \\ 0, & x(n) < 0 \end{Bmatrix}. \quad \textbf{(3)}$$

A cyclic prefix (CP) is then added to the beginning of each OFDM symbol to eliminate the ISI from the previous symbol, and the signal is parallel to serial converted into a single signal stream modulating the WLED intensity through the AWGN channel.

It is shown in [27] that the clipping noise due to the negative portion of the signal affects only the unused even subcarriers, while the odd data subcarriers remain unaffected except for an amplitude reduction to the half. So, the Rx can reconstruct the original message imposed on the odd data subcarriers without suffering from clipping noise.

Although ACO-OFDM is straightforward and characterized by higher power efficiency compared to DCO-OFDM [27], it suffers from a reduction in the channel spectral efficiency (SE) as the HS requirements put some constraints on the data subcarriers, where only N/2 data subcarriers are modulated; only half of them are reserved for effective data transmission as indicated by Eq. (1).

A number of solutions were discussed in literatures to increase the SE of ACO-OFDM based upon utilizing the unused even subcarriers to transmit data through the hybrid combination with other techniques of O-OFDM. This includes asymmetrically clipped DCO-OFDM (ADO-OFDM) [28], hybrid ACO-OFDM (HACO-OFDM) [29], and spectral and energy efficient OFDM (SEE-OFDM) [30]. A further design was described in [31], LACO-OFDM, which successively fills the unused even subcarriers with ACO-OFDM symbols through multiple layers. LACO-OFDM is characterized by its flexibility, since the number of layers, modulation order, and power allocated to each layer can be adjusted as required [32].

In LACO-OFDM, the transmitted signal is divided among L-layers. In each layer, the signal is applied to an ACO-OFDM modulator as described in Fig. 1. The first layer represents conventional ACO-OFDM, in which only the N/2 odd data subcarriers are utilized for data transmission, while the even data subcarriers are left unused.

In layer-2 and successive layers, the even data subcarriers are filled such that the unused subcarriers from previous layers are utilized, and the occupied subcarriers increase with each layer by $N/2^l$. In each layer, the unused subcarriers left from previous layers are used to carry data following the HS constraints, as depicted in Fig. 1. The sets of layer-l subcarriers carrying data are given by [33]

$$K_D^l = \left\{ 1 \times 2^{l-1}, 3 \times 2^{l-1}, 5 \times 2^{l-1}, \ldots\ldots, N - 2^{l-1} \right\},$$

$$1 \leq l \leq \log_2 N - 1. \quad \textbf{(4)}$$

It is shown in [31] that the time-domain signal at the IFFT output, $x^l(n)$, of layer-l follows a half-wave symmetry, such that [31]
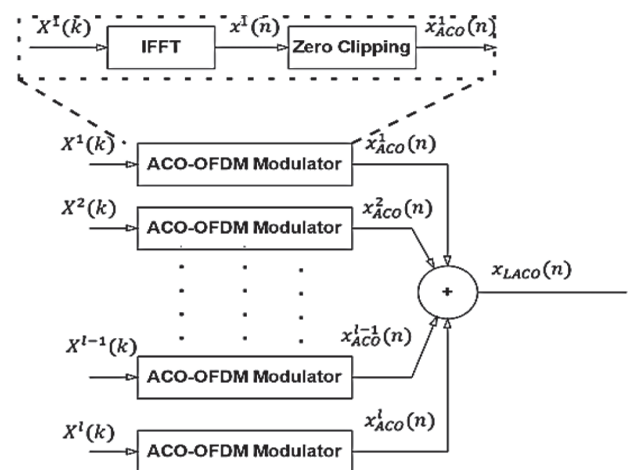

Fig. 1. Block diagram of LACO-OFDM indicating the arrangement of data subcarriers in different layers.

Table 1.   Iterative Rx Algorithm Adopted by LACO-OFDM [33][a]

Input: received symbols Y_k
Output: $\hat{X}_{D,k}^{(l)}$

1. **for** $l = 1 : L$ do
2.   **if** $l = 1$
3. $\check{X}_{D,k}^{(l)} = Y_k,\ k \in K_D^l$;
4.   **else**
5. $\check{X}_{D,k}^{(l)} = Y_k - \sum_{i=1}^{l-1} \check{X}_C^i(k),\ k \in K_D^l$;
6.   **end**
7. $\hat{X}_{D,k}^{(l)} = \arg \min_{X \in \Im_{M-QAM}} |2\check{X}_{D,k}^{(l)} - X|,\ k \in K_D^l$;
8. $x_{D,n}^{(l)} = \frac{1}{\sqrt{N}} \sum_{k \in K_D^l} \hat{X}_{D,k}^{(l)} \exp(\frac{j2\pi nk}{N})$;
9. $\hat{X}_{c,k}^{(l)} = \frac{1}{\sqrt{N}} \sum_{n=0}^{N-1} |x_{D,n}^{(l)}| \exp(\frac{-j2\pi nk}{N})$;
10. **end for**
11. **return** $\hat{X}_{ACO,k}^{(l)}$;

[a]Y_k denotes the received LACO-OFDM symbol in the frequency domain. $\hat{X}_{D,k}^{(l)}$ and $\hat{X}_{D,n}^{(l)}$ are the estimates of the transmitted data in the frequency domain and time domain for layer-l, respectively, while $\hat{X}_{c,k}^{(l)}$ is the corresponding clipping noise imposed by layer-l.

$$x^l(n) = -x^l\left(n + \frac{N}{2^l}\right), \quad n = 0, 1, 2, \ldots, \frac{N}{2^l} - 1. \quad \textbf{(5)}$$

Thus, the bipolar signal at each layer can be clipped without loss of information, and the clipping noise will fall into the even-indexed subcarriers given by [33]

$$K_c^l = \left\{K - 2^{l-1} : K \in K_D^l\right\}. \quad \textbf{(6)}$$

It is apparent that the clipping noise at each layer will not affect the current layer, but higher-order layers. Thus, an iterative Rx is used that iteratively decodes the lower-order layers, estimates the clipping noise, and subtracts it from the received data to find the data sent by the higher-order layers. The algorithm followed by the iterative Rx to decode the LACO-OFDM symbol is listed in Table 1.

3. IMPACT OF LED NONLINEARITY ON LACO-OFDM

In VLC systems, LEDs are considered as the main source of nonlinearity. LEDs suffer from a sharp decrease in quantum efficiency while increasing the injected current, which is referred to as "efficiency droop" [20], where the number of emitted photons is not proportional to the injected current. Taylor series expansion is a common approach to model the LED output power [6]:

$$P_{out}(t) = \sum_{n=0}^{\infty} \beta_n [I(t) - I_{DC}]^n, \quad \textbf{(7)}$$

where β_n represents the coefficient of the nth-order power of the polynomial model, and I_{DC} is the bias current.

High-order polynomial terms induce harmonics at higher frequency components and give rise to intermodulation distortion. At $n = 2$, LED nonlinearity produces harmonics at $2f_i$ and intermodulation products at $f_i + f_j$ and $f_i - f_j$ [6].

Table 2.   Simulation Model Parameters

LACO-OFDM	
No. of layers	4
IFFT length	256
No. of data subcarriers	240
CP length	0
LED (Cree PLCC4) [25]	
DC term (β_0)	-0.0628
Linear gain (β_1)	1.9472
Second-order nonlinear coefficient (β_2)	-0.8940
Turn-on voltage (TOV)	2.8 V
Maximum forward voltage	3.8 V
Maximum permissible AC/pulsed current	100 mA

Throughout this work, a polynomial of second-order degree ($n = 2$) is used to model the commercial WLED (Cree PLCC4) characteristics for two reasons. First, it provides a good agreement with the measured ($L - I$) values [5]. Second, the majority of the nonlinear distortion is subjected to the second-order term, while that of higher-order terms is negligible [6].

To distinguish the detrimental effect of LED nonlinearity and clipping distortion, the performance of LACO-OFDM is investigated taking into consideration the LED nonlinear ($L - I$) characteristics while assuming a linear ($I - V$) relationship. The LED $I - V$ characteristics are listed in Table 2 and are used to define the requirements of proper LED operation. The dynamic range of the LED is from a TOV of 2.8 V (corresponding to 0 A) to 3.8 V (100 mA). Note that out of 256 subcarriers, 240 of them are used in all layers compared to only 128 in the case of ACO-OFDM. All the data subcarriers in different layers are modulated with the same modulation order, and the conducted results are averaged over 4000 OFDM symbols.

According to Eq. (4), the maximum number of layers is seven. Although a higher number of layers means a higher SE, the improvement may be not significant when the number of layers is too large. Also, considering the constraints of either the electrical power or optical power, more layers usually lead to less power distributed to each layer, which may cause degradation to the system performance [34]. In this work, four layers out of seven are chosen for two reasons:

(1) more than 90% of the total subcarriers are utilized (93.75%);
(2) four layers provide the optimum performance at an adequate level of complexity, and as far as we know, it is considered in most of literatures dealing with LACO-OFDM.

Figure 2 shows the system performance at different SNR values assuming linear and nonlinear LED models. By default, the BER curve worsens while increasing the QAM level, as the constellation points become closer keeping the same noise level. LED nonlinearity distorts the signal and shifts the curves towards higher BER values compared to the linear LED model.

Naturally, this deviation becomes clearer at high SNR regions, where the noise contribution fades and the dominant source of distortion is due to LED nonlinearity as opposed to
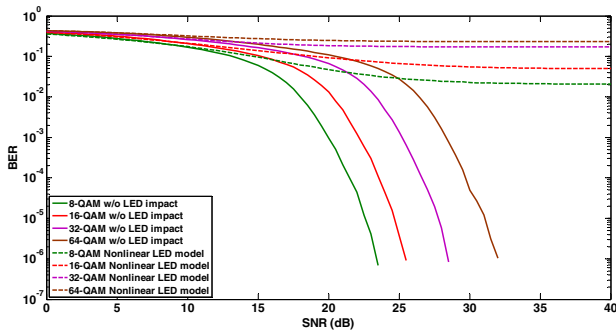
Fig. 2. BER at different SNRs considering linear and nonlinear LED models.

Fig. 4. BER at different bias voltage values.

low SNR regions, where the channel noise is dominant and affects both models' performances. The most important note is that in all cases and in the nonlinear LED model, the distortion caused by nonlinear LED response imposes a limit on the achieved system BER, and the recorded BER is higher than 10^{-2}.

An important factor that greatly determines the amount of clipping distortion imposed on the input signal is the input signal power values. Figure 3 depicts system performance at different OFDM signal powers. The average electrical power of the input signal is varied from 0 dBm to 30 dBm with an AWGN power of -10 dBm.

It can be seen that at low power regions, the SNR is low and the channel noise greatly affects system performance, while the nonlinear distortion is negligible. On the contrary, increasing the transmitted signal amplitude will counteract the channel noise effect, but the induced harmonic amplitudes will be enhanced, and the LED nonlinear distortion accumulates, leading to system BER deterioration. A further increase in signal power will push the signal into the saturation level and more peaks will be clipped. So, the system will not be able to transmit any meaningful message, especially in the case of higher-order QAM levels.

Thus, there is an optimum power value that guarantees a reasonable SNR level and produces the lowest achievable nonlinear distortion. However, even while transmitting with the optimum power value, system performance is greatly deteriorated, and the BER floor is still high, as indicated by Fig. 3.

Also, a proper choice of the bias voltage is an important step to reduce LED nonlinear effects by operating the LED in a quasi-linear segment of its $(L - I)$ characteristics. Figure 4 shows the
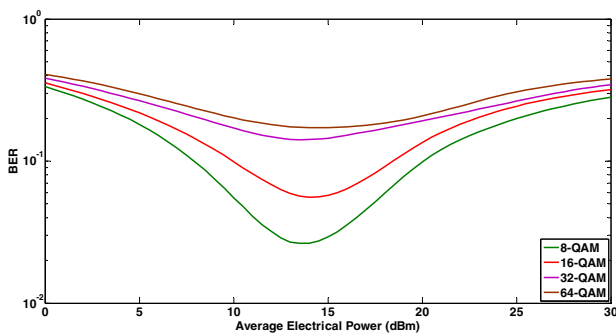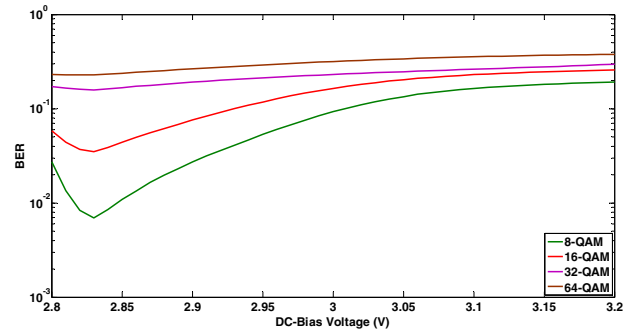
system performance at different bias voltage values. The values of bias voltage are varied from a TOV of 2.8 V (0 A) to 3.2 V, which corresponds to the maximum DC current (40 mA).

In Figs. 3 and 4, it is apparent that both the input signal power and DC-bias voltage shape the amount of induced nonlinear distortion added to the transmitted signal. Also, even in the case of operating with the optimum power and at the optimum DC-bias voltage, system performance is greatly deteriorated. In the case of 8-QAM and 16-QAM, the BER floor is higher than 10^{-3} and 10^{-2}, respectively, while the situation will be more severe at higher QAM orders. Thus, linearization of LED characteristics using predistorters or postdistorters is a vital solution to overcome the effects of LED nonlinear distortion and enhance system performance.

4. DIGITAL PREDISTORTER WITH POLYNOMIAL MODEL

The main idea of a digital predistorter is to define the LED nonlinear characteristics and find the inverse nonlinear LED coefficients such that the cascaded response of the predistorter and the LED is linear. Figure 5 illustrates the operation of the predistorter. A number of sampled data from the LED output after O/E conversion are fed back as the input of the predistorter to update its coefficients based upon the LS method. Then, the predistorter output is fed into the LED input.

Afterwards, the linear output of the LED is estimated and evaluated based on a given criterion such as a targeted BER or EVM. Based on the measured error, a decision is made such that the process is stopped or the coefficients of the predistorter are updated through repetition of the system operation. LED characteristics may change due to temperature and aging [35]. If the LED characteristics are changed, the algorithm modifies the predistorter coefficients to cope with the variations in the LED nonlinear behavior [15].

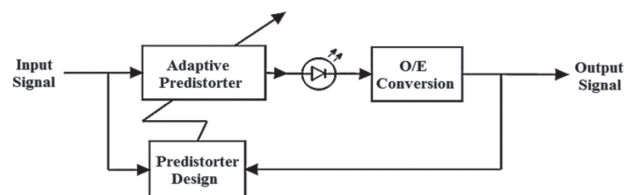The predistorter coefficients are calculated using the LS method [15]:

Fig. 3. BER at different electrical powers in presence of LED nonlinear distortion.

Fig. 5. Predistortion structure.

$$c_p = \left(Y^H Y\right)^{-1} Y^H V, \tag{8}$$

where P is the polynomial order, V is an $N \times 1$ output matrix, Y is an $N \times P$ input matrix, and $\hat{c}_p$ is a $P \times 1$ coefficient matrix. The efficiency of the proposed method is evaluated and tested with a polynomial order (P) of three at different bias points as shown in Fig. 6. The simulation results are conducted at different transmitted powers. Note that signal powers introducing high BER values are not plotted for the sake of figure clarity.

The results show that the BER can be neglected in the case of 64-QAM when applying the proposed method compared to a BER of 10^{-1} when there is no compensation technique, as shown in Figs. 3 and 4. The upcoming results will focus on 64-QAM, as it represents the worst case scenario, and by nature, all lower QAM orders will be enhanced accordingly. The optimal point for operation is at a DC-bias voltage of 3 V when the signal power is 15 dBm. Discontinuity in the BER curve indicates that the BER value at these points is negligible.

To understand, Fig. 7 shows the linearized LED model after adopting predistortion. It is apparent that at current values lower than 20 mA (corresponding to 3 V), the LED nonlinear response is still not completely compensated for, and so the BER is high, especially at 0 A (TOV), while values higher than the optimum will push the signal towards saturation regions and more peaks will be clipped.

The BER is a straightforward criterion to assess the system's performance through a one-to-one binary decision as to whether a bit is erroneous or not. EVM, on the other hand, is a measure of the differences between the measured and the expected symbols to infer the reception at the Rx earlier than the
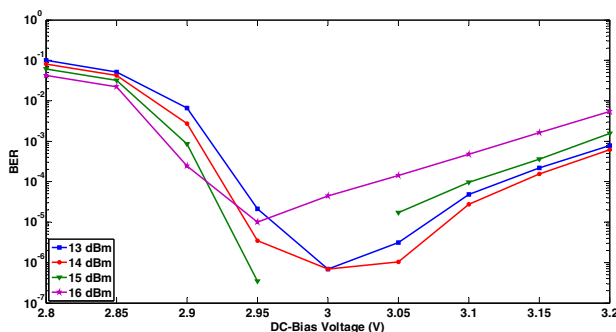

Fig. 6.   BER at different DC-bias voltages in the case of 64-QAM at SNR of 40 dB using polynomial-based predistorter.
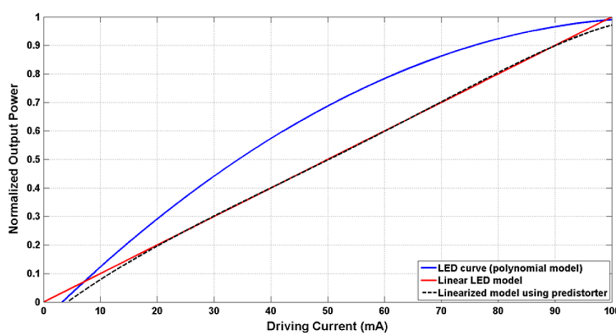

Fig. 7.   LED $(L - I)$ characteristics showing the linearized curve when using the polynomial-based predistorter.
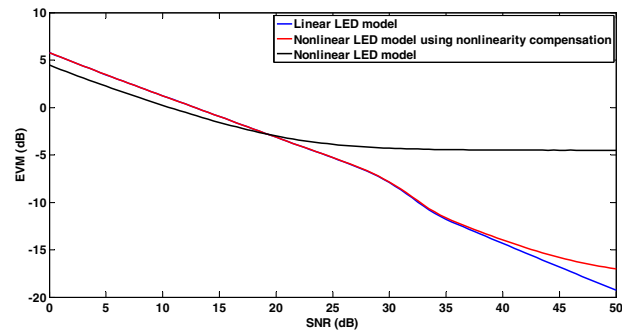

Fig. 8.   EVM at different SNR values with and without applying the polynomial-based predistortion technique.

end-to-end comparison through the BER and so saving extra calculations [36].

Figure 8 shows the EVM at different SNR values with and without applying the predistortion compensation technique. EVM represents the root mean square value of the error vector over time [9]. The error vector represents the deviation between the constellation points of the received and original symbols and can be expressed by [17]

$$\text{EVM} = \frac{\sqrt{\frac{1}{N} \sum_{k=0}^{N-1} \left((I(y_k) - I(x_k))^2 + (Q(y_k) - Q(x_k))^2 \right)}}{\sqrt{\frac{1}{N} \sum_{k=0}^{N-1} \left((I(x_k))^2 + (Q(x_k))^2 \right)}}, \tag{9}$$

where $(I(x_k), Q(x_k))$ and $(I(y_k), Q(y_k))$ represent the in-phase and quadrature constellation points at the kth subcarrier of the ideal and observed symbols, respectively.

It is apparent that LED nonlinearity greatly affects system performance and produces high EVM values even at higher SNR regions, as LED nonlinearity still imposes constraints on system performance at high SNR regions. On the other hand, LED nonlinearity distortion can be greatly alleviated using the proposed method; the EVM performance can be enhanced accordingly, and system performance becomes close to the linear LED model.

At regions of low SNR, the noise effect is dominant, and system performance is limited at these regions even in the case of the linear LED model. But when moving towards higher SNR, the noise effect fades away, the predistorter efficiency becomes clearer, and the performance of the system is close to that of the linear LED model.

The BER performance reflects the distribution of the EVM as depicted in Fig. 9. Up to a SNR of 30 dB, the system performance is limited under the noise effect. At higher values of SNR, the BER curve has a sharp decrease towards low BER values. At a targeted BER of 10^{-3}, only an extra 0.25 dB SNR is required to achieve the same BER compared to the linear LED model.

5. DIGITAL PREDISTORTER USING LUTs

In a LUT as illustrated by Fig. 10, the inverse of the LED nonlinear characteristics (F_i) is stored in a set of (N_T) LUT cells. The input signal (x_i) is assigned to the nearest cell and predistorted by multiplying the signal with the corresponding cell gain $(x_{\text{in\_pd}} = F_i x_{\text{in}})$, such that the cascaded response of the LUT and LED is linear.
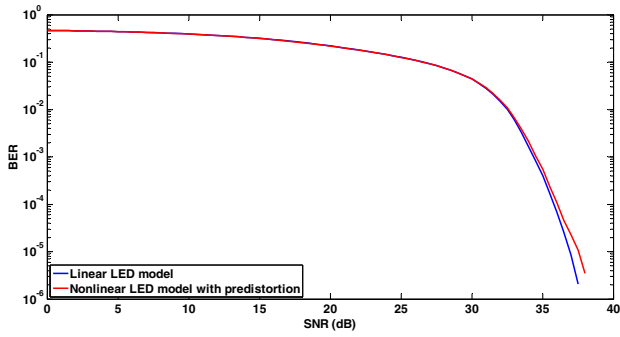
Fig. 9. BER performance indicating the impact of LED nonlinearity mitigation using polynomial-based predistorter.
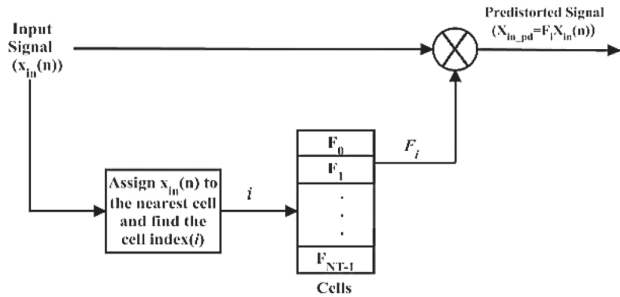

Fig. 10. Structure of the LUT-based predistorter [19].

To minimize the quantization error, the predistorter gain (F_i) of the cell should be chosen carefully to minimize the quantization error over the range of input signals to that cell. Based on this criterion, the predistorter gain (F_i) of each cell will be calculated according to an optimum input (x_{in}^*) that ensures a minimum quantization error over the entire cell. The optimum input (x_{in}^*) is found to be the mean value of the input signals to the cell [19]. Table 3 summarizes the procedures followed by the LUT predistorter to calculate the optimum gains. Note that this process is repeated at the beginning of data transmission to update the LUT entries to cope with variations in LED characteristics due to temperature or aging.

To evaluate the performance of the LUT-based predistorter when applied to a number of LEDs with different characteristics, the amplitude variations due to the nonlinear LED model are plotted in Figs. 11 and 12, assuming different LED ($L - I$) responses. The nonlinearity parameter, ζ, specifies how severe the LED's nonlinearity is. It has the following relationship with the coefficients of the LED transfer function's second-order polynomial model [6]:

$$\beta_0 = \zeta, \tag{10}$$

$$\beta_1 = 1, \tag{11}$$

$$\beta_2 = -4\zeta + 2. \tag{12}$$

LEDs are devices with a concave transfer function, whose ζ ranges from 0.5 to 0.75 depending on the LED type. A larger number of ζ implies a high degree of LED curvature and so severe nonlinear effects. The response of the LED approaches

Table 3. Algorithm for Calculating the Optimum Predistorter Gain (F_i) in the LUT-based Predistorter [19]

1. $x_{LED} = x_{min}$;
2. **for** $i = 0 : N_T - 1$
3. $x_{in}^* = x_{min} + (i + 0.5) \cdot D$; $D = (x_{max} - x_{min})/N_T$
4.   **if** ($x_{in}^* \leq LED$ saturation level)
5. $y_{out\_pd}^* = k x_{in}^*$; $k \ldots$ desired linear response slope
6.   **else**
7. $y_{out\_pd}^* = y_{max}$;
8.   **end**
9.   Find the LED output, y_{LED}, corresponding to x_{LED} using Eq. (7);
10. $x_{in\_pd} = x_{LED}$;
11.   Calculate the error, $r_{min} = |y_{LED} - y_{out\_pd}^*|$;
12.   **while** (**true**)
13. $x_{LED} = x_{LED} + \Delta$; $\Delta \ldots$ step size
14.   Calculate y_{LED} using Eq. (7);
15.   **if** $|y_{LED} - y_{out\_pd}^*| < r_{min}$
16. $r_{min} = |y_{LED} - y_{out\_pd}^*|$;
17. $x_{in\_pd} = x_{LED}$;
18.   **else**
19. $F_i = x_{in\_pd}/x_{in}^*$;
20.   **break**
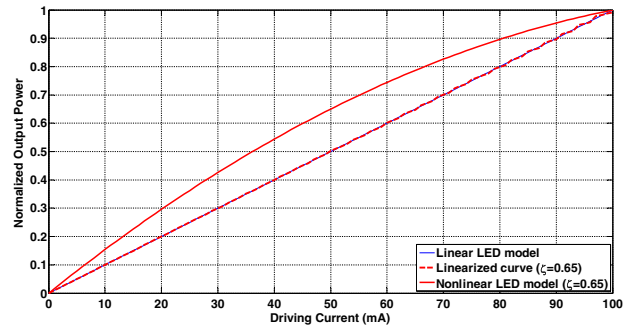21.   **end**
22.   **end**
22. **end**

Fig. 11. Variation of LED nonlinearity ($L - I$) response when applying the LUT-based predistorter with 32 cells at $\zeta = 0.65$.
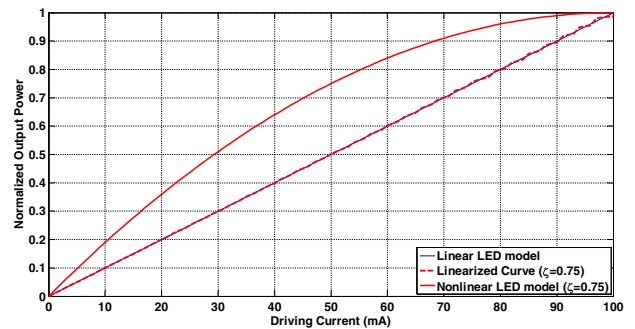

Fig. 12. Variation of LED nonlinearity ($L - I$) response when applying the LUT-based predistorter with 32 cells at $\zeta = 0.75$.

the linear LED model in the presence of a LUT-based predistorter in the case of $\zeta = 0.65$ and even at the worst case scenario, $\zeta = 0.75$. Thus, the proposed LUT-based predistorter is adequate in reducing the nonlinearity induced by various
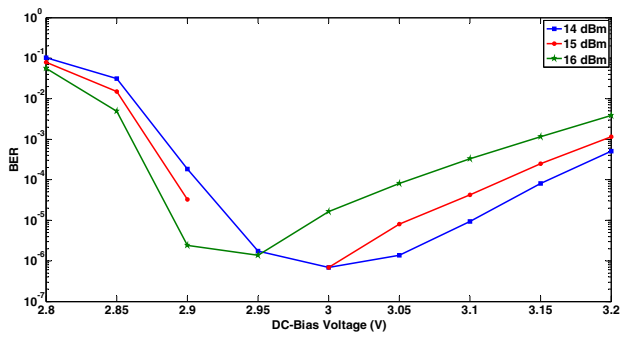
Fig. 13. BER at different DC-bias voltages in the case of 64-QAM at SNR of 40 dB and $N_T = 16$ using LUT predistorter.

Fig. 15. Effect of the number of LUT cells on the system EVM at different values of SNR using LUT-based predistorter.

Fig. 16. Impact of k-values on the performance of the system.

LEDs and can compensate for LED nonlinearity in different situations.

With $N_T = 16$ and $k = 1$, Fig. 13 shows the influence of varying the DC-bias voltage on system performance at different power values. It can be observed that the optimum operation is achieved at a DC-bias voltage of 2.95 V when the transmitted signal power is 15 dBm. Curve discontinuity at these values indicates that the LUT-based predistorter can achieve an error-free system.

The size of the LUT affects the amount of quantization error imposed on the applied signal and influences overall system performance, as shown in Fig. 14. When the number of LUT cells is eight, the recorded BER is settled around a value of 10^{-5} at high SNR regions, while system performance can be enhanced by using a larger number of cells.

Also, it can be observed that when the LUT consists of more than 32 cells, the added gain produced by increasing the number of cells is low compared to the negatives of adding extra cells such as complexity and time delay. Finally, when $N_T \geq 64$, the LUT predistorter performance is very close to the linear LED model with a SNR penalty of only 0.4 dB at a targeted BER of 10^{-5}. Figure 15 displays the corresponding EVM considering the effect of varying the number of the LUT cells.

The linear gain (k) produces a way to compromise between the dynamic range of the LED and the transmitted power. The linear gain can be selected to expand the dynamic range of the LED (2.8 V to 3.8 V) when operating with low values of k. On the other hand, the output power is proportional to the value of k, and cosequently, a lower value of k will produce lower output power.
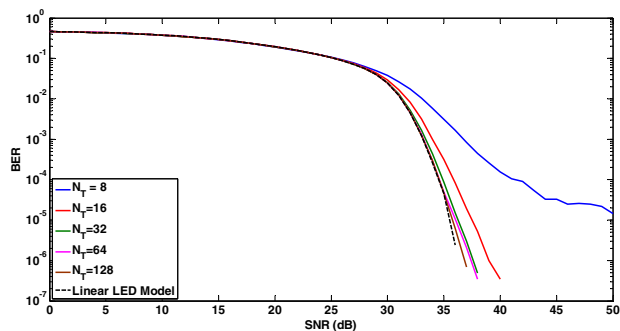

Fig. 14. Influence of varying the number of LUT cells on the performance of the system.
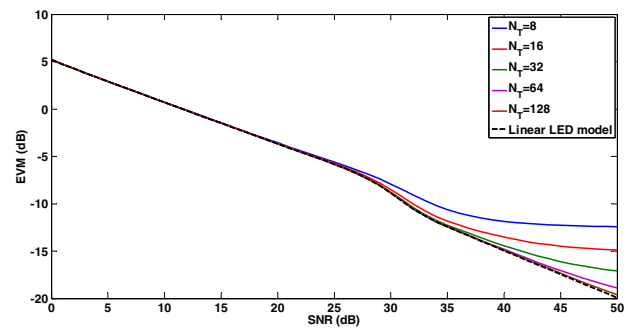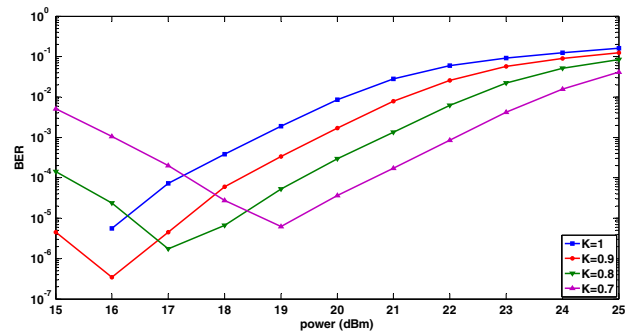
An increase in the transmitted power over the optimum one will deteriorate the system BER, as it will enhance the nonlinear components and push the signal towards the saturation region. One possible solution is to appropriately select a lower value of k to mitigate the nonlinearity effect at high signal power.

Figure 16 shows the impact of the k-values on system performance at different power values. It is clear that systems with lower values of k perform better at high power regions. For example, at 19 dBm, the recorded BER at $k = 0.7$ is 6.25×10^{-6} compared to a BER of 5×10^{-5}, 4×10^{-4}, and 2×10^{-3} in the case of $k = 0.8, 0.9$, and 1, respectively.

6. DIGITAL POSTDISTORTER

At the Rx side, a digital postdistorter is used to mitigate the LED nonlinearity effects and is inserted after the photodiode. The received optical signal is first O/E converted into the corresponding electrical signal, $y(n)$. It is then used with the corresponding training sequence, $x(n)$, to find the coefficients of the polynomial representing the inverse of the LED characteristics such that the output signal from the digital postdistorter is linear with the transmitted one, as shown in Fig. 17. The feedback is inserted to capture the changes in the LED characteristics and adapt the postdistortion coefficients to these variations.

The postdistorter output samples, $\hat{x}(n)$, are characterized by a nonlinear polynomial model given by [14]
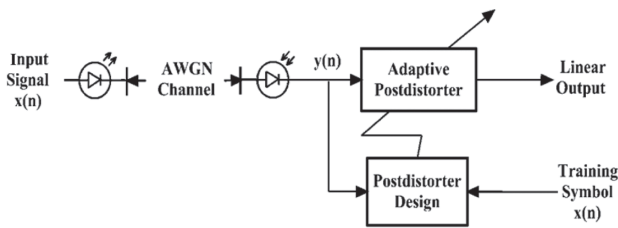
$$\hat{x}(n) = \sum_{p=0}^{P-1} C_p y^{p+1}(n), \tag{13}$$

Fig. 17. Block diagram of the digital postdistorter.

where C_p represents the coefficients of the postdistorter, and P is the number of polynomial terms.

Then, the error signal, $e(n)$, is given by [14]

$$e(n) = x(n) - \hat{x}(n) = x(n) - \sum_{p=0}^{P-1} C_p y^{p+1}(n). \quad \textbf{(14)}$$

The coefficients are chosen to minimize the power of the error signal. The objective function is given by [14]

$$\arg_c \min \sum_{n=0}^{N-1} |e(n)|^2 = \arg_c \min \sum_{n=0}^{N-1} |x(n)$$

$$- \sum_{p=0}^{P-1} C_p y^{p+1}(n)|^2. \quad \textbf{(15)}$$

The LS solution can be obtained as [14]

$$C = \left(Y^H Y\right)^{-1} Y^H X, \quad \textbf{(16)}$$

where C is the $P \times 1$ postdistortion coefficients vector, Y is the $N \times P$ received symbols matrix, X is the $N \times 1$ training symbols vector, and $(.)^H$ denotes the Hermitian transpose.

Figure 18 shows the system performance at different DC-bias voltage values when the transmitted power is varied for $P = 3$. It is apparent that nearly error-free performance can be obtained when the DC-bias points of operation are 2.9 V and 2.95 V. A signal power of 13 dBm and 14 dBm are the optimum signal powers.

The efficiency of the proposed method is evaluated and tested using EVM and BER calculations, as illustrated in Figs. 19 and 20, respectively. The results are conducted at a transmitted power of 13 dBm and a DC-bias voltage of 2.95 V. At low SNR regions, the noise effect is dominant, and the system suffers from performance degradation even in the case of the linear LED model.
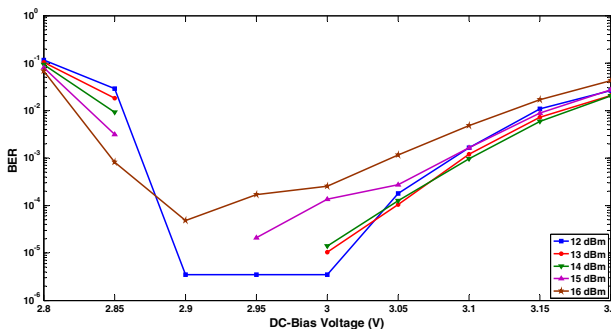

Fig. 18. Effect of bias voltage and transmitted signal power on the system performance using polynomial-based postdistorter.
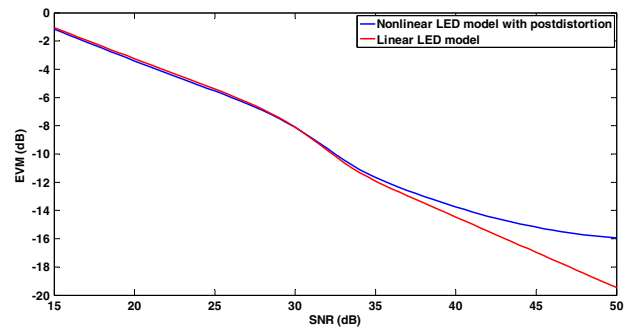

Fig. 19. EVM versus SNR showing the efficiency of the postdistortion technique compared to the linear LED model.
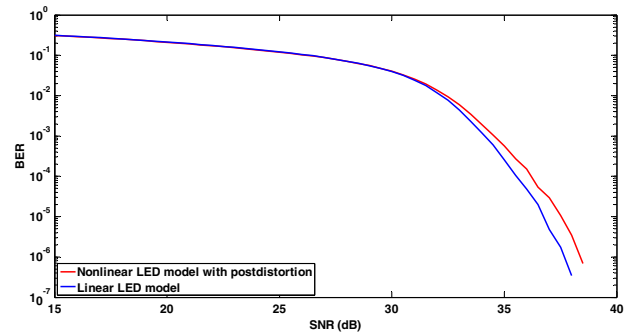

Fig. 20. BER versus SNR considering LED nonlinearity mitigation using postdistortion.

When SNR is higher than 25 dB, the BER decreases with an increasing rate. Results show that the proposed postdistorter is very successful in limiting the effects of LED nonlinearity, and the recorded BER values using the postdistorter are close to that of the linear LED model. It requires an extra SNR of only 0.25 dB to achieve a BER of 10^{-3} in the case of using a postdistorter compared to the linear LED model.

7. CONCLUSION

LED represents the main source of nonlinearity in VLC-based systems. The detrimental effect of LED nonlinearity limits the overall system performance and imposes some constraints on the achieved BER. In LACO-OFDM and when considering the adverse effect of LED nonlinearity, the BER floor is higher than 10^{-2} in the case of different QAM orders.

The appropriate choice of DC-bias voltage and signal power is an important step to alleviate the impact of LED nonlinearity through operating the LED in a quasi-linear region of its characteristics far away the high power regions characterized by high nonlinear distortion and low power regions characterized by low SNR. However, this step is not enough, as the LED is characterized by strong nonlinearity.

Predistortion and postdistortion are effective techniques to overcome LED nonlinear distortion through linearizing the overall system response. Generally, both can be established based on the polynomial model or LUT.

In this paper, three compensation techniques are evaluated and tested to mitigate LED nonlinearity in four-layer LACO-OFDM. The first is a predistorter based on a polynomial model

whose coefficients can be calculated using the LS method. It requires an extra SNR of 0.25 dB to achieve a BER of 10^{-3} compared to the linear LED model in the case of 64-QAM. Based on the second technique, a LUT-based predistorter is used to compensate for LED nonlinearity. The obtained results show that the LUT-based predistorter is very close to the performance of the linear LED model when the number of cells is larger than 64. The last technique is a postdistorter whose coefficients can be determined using the LS method. It requires an extra SNR of only 0.25 dB to achieve a BER of 10^{-3} compared to the linear LED model in the case of 64-QAM.

To sum up, digital predistortion and postdistortion techniques accompanied with proper DC-bias voltages and transmitted signal power can completely compensate for the impact of LED nonlinearity in LACO-OFDM. The LUT-based predistorter produces the most remarkable performance among the mentioned ones. However, the performance of the LUT-based predistorter depends on the number of LUT cells, and consequently, a highly efficient LUT predistorter requires a large number of cells at the expense of increased complexity. On the other hand, polynomial-based predistorters and postdistorters require an extra SNR of only 0.25 dB to achieve the same BER as the linear LED model with reduced complexity.

As a future direction, these techniques are to be extended to different LACO-OFDM modified Rxs including diversity combining and noise-cancellation-based Rxs with more insight into computational complexity. In addition, it will be interesting to develop the LED model as a nonlinear system with memory effects that incorporate the frequency response of the LED showing the corresponding effects with possible solutions.

Disclosures.   The authors declare no conflicts of interest.

Data Availability.   Data underlying the results presented in this paper are not publicly available at this time but may be obtained from the authors upon reasonable request.

REFERENCES

1. H. Haas, "LiFi is a paradigm-shifting 5G technology," Rev. Phys. **3**, 26–31 (2018).
2. M. Elkarim, N. Mohammed, and M. Aly, "Exploring the performance of indoor localization systems based on VLC-RSSI, including the effect of NLOS components using two light-emitting diode lighting systems," Opt. Eng. **54**, 105110 (2015).
3. R. Mesleh, H. Elgala, and H. Haas, "On the performance of different OFDM based optical wireless communication systems," J. Opt. Commun. Netw. **3**, 620–628 (2011).
4. N. A. Mohammed, M. M. Elnabawy, and A. A. M. Khalaf, "PAPR reduction using a combination between precoding and non-linear companding techniques for ACO-OFDM-based VLC systems," Opto-Electron. Rev. **29**, 59–70 (2021).
5. M. Abd Elkarim, M. M. Elsherbini, H. M. AbdelKader, and M. H. Aly, "Exploring the effect of LED nonlinearity on the performance of layered ACO-OFDM," Appl. Opt. **59**, 7343–7351 (2020).
6. B. Inan, S. C. Jeffrey Lee, S. Randel, I. Neokosmidis, A. M. J. Koonen, and J. W. Walewski, "Impact of LED nonlinearity on discrete multitone modulation," J. Opt. Commun. Netw. **1**, 439–451 (2009).
7. I. Neokosmidis, T. Kamalakis, J. W. Walewski, B. Inan, and T. Sphicopoulos, "Impact of nonlinear LED transfer function on discrete multitone modulation: analytical approach," J. Lightwave Technol. **27**, 4970–4978 (2009).
8. H. Elgala, R. Mesleh, and H. Haas, "An LED model for intensity-modulated optical communication systems," IEEE Photon. Technol. Lett. **22**, 835–837 (2010).
9. H. Elgala, R. Mesleh, and H. Haas, "A study of LED nonlinearity effects on optical wireless transmission using OFDM," in *IFIP International Conference on Wireless and Optical Communications Networks* (2009), pp. 1–5.
10. V. K. Singh and U. D. Dalal, "Investigation of LED non-linearity on DCO-OFDM and ACO-OFDM in VLC systems using multichip RGB LEDs for indoor applications," Proc. Comput. Sci. **143**, 852–859 (2018).
11. Z. Yu, R. J. Baxley, and G. T. Zhou, "EVM and achievable data rate analysis of clipped OFDM signals in visible light communication," EURASIP J. Wireless Commun. Netw. **2012**, 321 (2012).
12. D. Tsonev, S. Sinanovic, and H. Haas, "Complete modeling of non-linear distortion in OFDM-based optical wireless communication," J. Lightwave Technol. **31**, 3064–3076 (2013).
13. H. Elgala, R. Mesleh, and H. Haas, "Non-linearity effects predistortion in optical OFDM wireless transmission using LEDs," Int. J. Ultra Wideband Commun. Syst. **1**, 143–150 (2009).
14. H. Qian, S. J. Yao, S. Z. Cai, and T. Zhou, "Adaptive postdistortion for nonlinear LEDs in visible light communications," IEEE Photon. J. **6**, 1–8 (2014).
15. J. K. Kim, K. Hyun, and S. K. Park, "Adaptive predistorter using NLMS algorithm for nonlinear compensation in visible-light communication system," Electron. Lett. **50**, 1457–1459 (2014).
16. J. Li, Z. Huang, X. Liu, and Y. Ji, "Hybrid time-frequency domain equalization for LED nonlinearity mitigation in OFDM-based VLC systems," Opt. Express **23**, 611–619 (2015).
17. P. Aggarwal, T. Kabra, R. Ahmad, V. A. Bohara, and A. Srivastava, "Adaptive learning architecture-based predistorter for nonlinear VLC system," Photon. Netw. Commun. **38**, 258–269 (2019).
18. R. Mitra and V. Bhatia, "Chebyshev polynomial-based adaptive predistorter for nonlinear LED compensation in VLC," IEEE Photon. Technol. Lett. **28**, 1053–1056 (2016).
19. J. Sheu, B. Li, and J. Lain, "LED non-linearity mitigation techniques for optical OFDM-based visible light communications," IET Optoelectron. **11**, 259–264 (2017).
20. H. Lu, J. Jin, and J. Wang, "Alleviation of LED nonlinearity impact in visible light communication using companding and predistortion," IET Commun. **13**, 818–821 (2019).
21. C. Chen, X. Deng, Y. Yang, P. Du, H. Yang, and L. Zhao, "LED nonlinearity estimation and compensation in VLC systems using probabilistic Bayesian learning," Appl. Sci. **9**, 2711 (2019).
22. J. Ma, J. He, J. Shi, J. He, Z. Zhou, and R. Deng, "Nonlinear compensation based on K-means clustering algorithm for Nyquist PAM-4 VLC system," IEEE Photon. Technol. Lett. **31**, 935–938 (2019).
23. X. Lu, K. Wang, L. Qiao, W. Zhou, Y. Wang, and N. Chi, "Nonlinear compensation of multi-CAP VLC system employing clustering algorithm based perception decision," IEEE Photon. J. **9**, 1–9 (2017).
24. X. Lu, C. Lu, W. Yu, L. Qiao, S. Liang, A. P. T. Lau, and N. Chi, "Memory-controlled deep LSTM neural network post-equalizer used in high-speed PAM VLC system," Opt. Express **27**, 7822–7833 (2019).
25. P. Miao, B. Zhu, C. Qi, Y. Jin, and C. Lin, "A model-driven deep learning method for LED nonlinearity mitigation in OFDM-based optical communications," IEEE Access **7**, 71436–71446 (2019).
26. Y. Sun, F. Yang, and J. Gao, "Comparison of hybrid optical modulation schemes for visible light communication," IEEE Photon. J. **9**, 1–13 (2017).
27. J. Armstrong and A. J. Lowery, "Power efficient optical OFDM," Electron. Lett. **42**, 370–372 (2006).
28. S. D. Dissanayake and J. Armstrong, "Comparison of ACO-OFDM, DCO-OFDM and ADO-OFDM in IM/DD systems," J. Lightwave Technol. **31**, 1063–1072 (2013).
29. B. Ranjha and M. Kavehrad, "Hybrid asymmetrically clipped OFDM-based IM/DD optical wireless system," J. Opt. Commun. Netw. **6**, 387–396 (2014).
30. H. Elgala and T. D. C. Little, "SEE-OFDM: spectral and energy efficient OFDM for optical IM/DD systems," in *IEEE 25th Annual International Symposium on Personal, Indoor, and Mobile Radio Communication (PIMRC)* (2014), pp. 851–855.

31. Q. Wang, C. Qian, X. Guo, Z. Wang, D. G. Cunningham, and I. H. White, "Layered ACO-OFDM for intensity-modulated direct-detection optical wireless transmission," Opt. Express **23**, 12382–12393 (2015).

32. X. Zhang, Q. Wang, R. Zhang, S. Chen, and L. Hanzo, "Performance analysis of layered ACO-OFDM," IEEE Access **5**, 18366–18381 (2017).

33. M. M. A. Mohammed, C. He, and J. Armstrong, "Diversity combining in layered asymmetrically clipped optical OFDM," J. Lightwave Technol. **35**, 2078–2085 (2017).

34. F. Yang, Y. Sun, and J. Gao, "Adaptive LACO-OFDM with variable layer for visible light communication," IEEE Photon. J. **9**, 1–8 (2017).

35. L. C. Mathias, J. C. Marinello Filho, and T. Abrao, "Predistortion and pre-equalization for nonlinearities and low-pass effect mitigation in OFDM-VLC systems," Appl. Opt. **58**, 5328–5338 (2019).

36. R. A. Shafik, M. S. Rahman, and A. R. Islam, "On the extended relationships among EVM, BER and SNR as performance metrics," in *International Conference on Electrical and Computer Engineering* (2006), pp. 408–411.